



Mathematical Modelling of Juxtacrine Patterning

H. J. WEARING

Department of Mathematics,
Heriot-Watt University,
Edinburgh EH14 4AS, U.K.

E-mail: helenw@ma.hw.ac.uk

M. R. OWEN

Department of Mathematics,
University of Utah,
Salt Lake City,
Utah 84112, U.S.A.

Department of Mathematical Sciences,
Loughborough University,
LE11 3TU, U.K.

E-mail: M.R.Owen@lboro.ac.uk

J. A. SHERRATT

Department of Mathematics,
Heriot-Watt University,
Edinburgh EH14 4AS, U.K.

E-mail: jas@ma.hw.ac.uk

Spatial pattern formation is one of the key issues in developmental biology. Some patterns arising in early development have a very small spatial scale and a natural explanation is that they arise by direct cell–cell signalling in epithelia. This necessitates the use of a spatially discrete model, in contrast to the continuum-based approach of the widely studied Turing and mechanochemical models. In this work, we consider the pattern-forming potential of a model for juxtacrine communication, in which signalling molecules anchored in the cell membrane bind to and activate receptors on the surface of immediately neighbouring cells. The key assumption is that ligand and receptor production are both up-regulated by binding. By linear analysis, we show that conditions for pattern formation are dependent on the feedback functions of the model. We investigate the form of the pattern: specifically, we look at how the range of unstable wavenumbers varies with the parameter regime and find an estimate for the wavenumber associated with the fastest growing mode. A previous juxtacrine model for Delta–Notch signalling studied by Collier *et al.* (1996, *J. Theor. Biol.* **183**, 429–446) only gives rise to patterning with a length scale of one or two cells, consistent with the fine-grained patterns seen in a number of developmental processes. However, there is evidence of longer range patterns in early development of the fruit fly *Drosophila*. The analysis we carry out predicts that patterns longer than one or two cell lengths are possible with our positive feedback mechanism, and numerical simulations confirm this. Our work shows that

juxtacrine signalling provides a novel and robust mechanism for the generation of spatial patterns.

© 2000 Society for Mathematical Biology

1. INTRODUCTION

Nearly all of the existing mathematical models for spatial pattern formation in developmental biology are based on continuum processes. However, the cellular diversity exhibited in early development does not appear on such a macroscopic scale. Indeed, why individual cells acquire specific fates is most likely to be a consequence of cellular interactions. Nearest-neighbour communication or juxtacrine signalling is one important way in which this is thought to occur. In this paper we develop a model that provides a novel and robust mechanism for patterning arising from nearest-neighbour interactions.

1.1. Continuum models for pattern formation. Reaction–diffusion systems have been a major focus of interest since Turing (1952) proposed the chemical pre-pattern approach in his seminal paper of 1952. He showed that, under certain conditions, chemicals can react and diffuse in such a way as to produce heterogeneous spatial patterns of chemical concentration. Once established, the pre-pattern is interpreted by the cells which then differentiate accordingly. Thus, once the initial pattern has been laid down, cellular development is independent of the pattern-generating mechanism. Turing systems have been applied to a large number of biological situations. For example, Kauffman *et al.* (1978) presented one of the first practical applications to early segmentation of the embryo of the fruit fly *Drosophila*, while Murray (1993) applied reaction–diffusion systems to animal coat patterns at the beginning of the 1980s. Recent work by Varea *et al.* (1997) has looked at the applications to skin patterns of some marine fish, considering a confined Turing system on a growing domain.

Most applications of the Turing theory have one common feature: they are considered in the context of a homogeneous environment where the model parameters are constant across the domain. However, as experimental evidence suggests, some embryological systems may exhibit environmental inhomogeneities. The form of Turing patterns in such cases was analysed by Benson *et al.* (1993). They considered a two-species reaction–diffusion system where the dispersal rate of one species varied in a simple step-wise manner, and discussed its application to the development of cartilage pattern in embryonic chick limb. More recently, Voroney *et al.* (1996) have investigated the interaction between oscillatory dynamics and Turing pattern formation in a heterogeneous environment. The importance of such work has been highlighted since the identification of Turing patterns in chemical systems, by Castets *et al.* (1990). Such chemical reactions have provided experimental observations that illustrate the interaction of Turing (spatial) and Hopf

(temporal) instabilities (Dulos *et al.*, 1996). A detailed review of the application of reaction–diffusion theory to chemical systems and its biological implications is given by Maini *et al.* (1997).

Mechanochemical theory has a much shorter history. Developed by Oster, Murray and colleagues in the early 1980s, mechanochemical models reflect the laws of mechanics as applied to tissue cells and their environment; an issue which is not addressed by pre-pattern models. All parameters involved are in principle measurable, since the models are based on specific biological and biochemical mechanisms. In contrast to Turing systems, there is no separation between the pattern formation and morphogenetic processes in mechanochemical mechanisms, enabling them to adjust to external disturbances. Mechanochemical models have been applied to a variety of patterning problems, such as feather germ primordia (Murray *et al.*, 1983) and cartilage formation in the vertebrate limb (Oster *et al.*, 1985). Recent work on wound-healing in mammalian skin is an important example of how the models can be adapted to obtain an understanding of morphogenesis in living tissue (Murray *et al.*, 1988; Olsen *et al.*, 1995).

Both the Turing and mechanochemical approaches are based on continuum models and this is not always biologically appropriate. In particular, some patterns arising in early development have a very small spatial scale; examples include mesoderm induction in *Xenopus* (Reilly and Melton, 1996) and the patterning in *Drosophila* imaginal discs (Serrano and O'Farrell, 1997). A natural explanation for such patterns is that they arise by direct cell–cell signalling in epithelia, a microscopic process, which necessitates the use of a spatially discrete model.

1.2. Juxtacrine signalling. Cellular communication has traditionally been divided into autocrine, paracrine and endocrine molecular activity. These mean respectively that the molecule acts only on the cell which secreted it, on neighbouring cells via extracellular diffusion, and on all cells within a tissue. However, within the close-packed cellular structure of epithelia another form of communication is possible: 'juxtacrine signalling'—as it was termed by Massagué (1990). In this process the signalling molecules anchored in the cell membrane bind to and activate receptors on the surface of immediately neighbouring cells. There are two main types of juxtacrine signalling molecules: (i) those that only exist in membrane-bound forms, for example the *Drosophila* proteins Boss and Delta which bind respectively to the receptors Sevenless and Notch (Lewis, 1996); (ii) those that are membrane-bound precursors of soluble paracrine ligands, such as epidermal growth factor (EGF) and the closely related transforming growth factor- α (TGF α) (Massagué, 1993). In the latter case, the relative rates of cleavage and decay of the membrane-bound form determine the relative importance of paracrine and juxtacrine signalling modes.

Collier *et al.* (1996) were the first to consider explicit mathematical modelling of juxtacrine communication when they investigated the pattern-forming potential of Delta–Notch signalling during *Drosophila* development. Their model incorporates

lateral inhibition; a type of cell–cell interaction whereby a cell fated in a particular way inhibits its neighbours from developing similarly. This is controlled by a negative feedback loop: the more inhibition a cell delivers to its neighbours, the less it receives back from them, and the more it is consequently able to deliver. The work by Collier *et al.* showed that, provided the feedback was sufficiently strong, such a nearest-neighbour lateral inhibition mechanism is capable of generating by itself the fine-grained patterns observed in early development. However, many membrane-bound growth factors act in a quite different way, by up-regulating their own production. Models that incorporate such positive feedback have been proposed in three recent papers studying juxtacrine signal range: Monk (1998) has adapted the Collier *et al.* model to study transforming growth factor- β (TGF β) juxtacrine signalling, with particular application to *Xenopus* mesoderm induction; whereas Owen and Sherratt (1998) and Owen *et al.* (1999) have investigated signal range in a more generic model for juxtacrine communication. In this work, we consider the pattern-forming potential of the model developed by Owen and Sherratt (1998), in which the key nonlinearity is a positive feedback loop.

In Section 2, we introduce the model equations and detail the main assumptions. Using linear analysis in Section 3, we derive conditions for pattern formation which are dependent on the feedback functions of the model. We then investigate the form of the pattern: in particular, we look at how the range of unstable wavenumbers varies with the parameter regime and find an estimate for the wavenumber associated with the fastest growing mode. In Section 4, we solve the model equations numerically to confirm and extend our results. The implications of this work and possible extensions are discussed in Section 5.

2. MATHEMATICAL MODEL

The mathematical model consists of a series of three coupled ordinary differential equations representing ligand–receptor binding, with one set of equations for each cell. We consider a two-dimensional epithelial sheet which is represented as a regular array of identical, square cells. For simplicity, we look at behaviour which is one-dimensional, with ligand and receptor levels varying only in one direction across this array of cells. The kinetic scheme we use is as generic as possible: we assume that a single ligand molecule binds reversibly to a receptor on the cell surface, giving an occupied receptor which is internalized within the cell. In practice, new ligand and new receptors will be produced at the cell surface through a combination of recycling, release from intracellular stores, and *de novo* production within the cell. This complex series of processes has been modelled explicitly in a few specific cases (Zigmond *et al.*, 1982; Martiel and Goldbeter, 1987), but the simplifying assumption here is that production of both ligand and receptor occurs at a rate that increases with the current level of occupied receptors. Such positive feedback is a central assumption in the model; it is well-documented for a number

of ligand–receptor interactions, including the binding of TGF α and EGF to the EGF receptor (EGF-R) in keratinocytes (Clark *et al.*, 1985; Coffey *et al.*, 1987).

Thus, the variables are the number of ligand molecules $a_j(t)$, free receptors $f_j(t)$ and bound receptors $b_j(t)$ on the surface of cells in row j (an integer) at time t . This gives the equations:

$$\frac{\partial a_j}{\partial t} = \underbrace{-k_a a_j \langle f_j \rangle}_{\text{binding}} + \underbrace{k_d \langle b_j \rangle}_{\text{dissociation}} - \underbrace{d_a a_j}_{\text{decay}} + \underbrace{P_a \langle b_j \rangle}_{\text{production}} \quad (1a)$$

$$\frac{\partial f_j}{\partial t} = -k_a \langle a_j \rangle f_j + k_d b_j - d_f f_j + P_f \langle b_j \rangle \quad (1b)$$

$$\frac{\partial b_j}{\partial t} = +k_a \langle a_j \rangle f_j - k_d b_j - \underbrace{k_i b_j}_{\text{internalization}} \quad (1c)$$

Here P_a and P_f represent the synthesis of new ligand and receptor molecules by epithelial cells. These are increasing functions of b_j , the number of bound receptors; the exact form of these functions will be discussed later. The notation $\langle \cdot \rangle$ reflects the juxtacrine communication, indicating an average over neighbouring cells. In the context of our assumption of a regular grid of square cells, this is defined by

$$\langle a_j \rangle \equiv \frac{a_{j-1} + 2a_j + a_{j+1}}{4}, \text{ etc.} \quad (2)$$

These terms represent the total number of ligand molecules, free and bound receptors available on the surface of the cells adjacent to those in row j . The term $2a_j$ enters because two of the four neighbours of any cell are in the same row, and are thus identical under our assumption of one-dimensional behaviour.

3. LINEAR ANALYSIS OF PATTERN FORMATION

We begin our study of the pattern-forming ability of the juxtacrine system by analysing the stability of a homogeneous steady state, denoting the equilibrium levels of ligand molecules and free and bound receptors by (a_e, f_e, b_e) . It is straightforward to show that there is always at least one such steady state. The trivial state, with $a = b = 0$, corresponding to the absence of any ligand binding at the cell surface, is not relevant to pattern formation, since oscillations about it are not possible. In this section we wish to investigate the temporal stability of the homogeneous equilibrium to spatially varying perturbations. We begin by linearizing the model (1a)–(c) about the homogeneous steady state, setting $a_j = a_e + \tilde{a}_j$, $f_j = f_e + \tilde{f}_j$, $b_j = b_e + \tilde{b}_j$, to give:

$$\frac{\partial \tilde{a}_j}{\partial t} = -k_a f_e \tilde{a}_j - k_a a_e \langle \tilde{f}_j \rangle + k_d \langle \tilde{b}_j \rangle - d_a \tilde{a}_j + \mathcal{A} \tilde{b}_j \quad (3a)$$

$$\frac{\partial \tilde{f}_j}{\partial t} = -k_a \langle a_j \rangle f_e - k_a a_e \tilde{f}_j + k_d \tilde{b}_j - d_f \tilde{f}_j + \mathcal{F} \tilde{b}_j \quad (3b)$$

$$\frac{\partial \tilde{b}_j}{\partial t} = +k_a \langle \tilde{a}_j \rangle f_e + k_a a_e \tilde{f}_j - k_d \tilde{b}_j - k_i \tilde{b}_j \quad (3c)$$

where $\langle \cdot \rangle$ is defined by (2). Here $\mathcal{A} = P'_a(b_e)$ and $\mathcal{F} = P'_f(b_e)$ are the slopes of the feedback functions at the steady state; we will show that these are the key parameters in the conditions for pattern formation. We look for solutions of the form $\tilde{a}_j = \bar{a} e^{\alpha t + i\lambda j}$ etc., where \bar{a} is an arbitrary constant, α is the temporal growth rate and λ is the wavenumber. Each of the averaged terms for the contribution of neighbouring cells is then of the form

$$\frac{(\tilde{a}_{j-1} + 2\tilde{a}_j + \tilde{a}_{j+1})}{4} = \bar{a} e^{\alpha t + i\lambda j} \frac{(e^{i\lambda} + 2 + e^{-i\lambda})}{4}$$

with a corresponding reduction for b and f . For notational simplicity, we define

$$K(\lambda) \equiv \frac{(e^{i\lambda} + e^{-i\lambda} + 2)}{4} = \frac{\cos(\lambda) + 1}{2}. \quad (4)$$

Substituting into the linearized model, dividing throughout by $e^{\alpha t + i\lambda j}$ and collecting the terms in matrix form gives:

$$\begin{pmatrix} k_a f_e + d_a + \alpha & k_a a_e K & -k_d K - \mathcal{A} \\ k_a f_e K & k_a a_e + d_f + \alpha & -k_d - \mathcal{F} \\ -k_a f_e K & -k_a a_e & k_d + k_i + \alpha \end{pmatrix} \begin{pmatrix} \bar{a} \\ \bar{f} \\ \bar{b} \end{pmatrix} = 0. \quad (5)$$

For nontrivial solutions we require the determinant of this matrix to be zero. Expanding the determinant gives a cubic characteristic equation, denoted by $P(\alpha)$, whose roots determine the stability of the steady state. $P(\alpha) = \alpha^3 + a_1 \alpha^2 + a_2(K)\alpha + a_3(K)$, where

$$a_1 = k_a a_e + k_a f_e + d_a + d_f + k_d + k_i \quad (6a)$$

$$a_2(K) = -K^2 k_a f_e (k_a a_e + k_d) - K k_a f_e \mathcal{A} + d_a d_f + (d_a + d_f)(k_d + k_i) + k_a f_e (k_a a_e + d_f + k_d + k_i) + k_a a_e (d_a + k_i - \mathcal{F}) \quad (6b)$$

$$a_3(K) = -K^2 k_a f_e [k_a a_e (k_i - \mathcal{F}) + k_d d_f] - K k_a f_e d_f \mathcal{A} + [k_a f_e + d_a][k_a a_e (k_i - \mathcal{F}) + d_f (k_d + k_i)]. \quad (6c)$$

For spatial pattern formation we require the steady state to be:

- stable to homogeneous perturbations
- and unstable to inhomogeneous perturbations;

we consider these conditions separately.

3.1. Stability to homogeneous perturbations. We first consider conditions for the stability of the steady state to homogeneous perturbations, which correspond to imposing $\lambda = 0$ (i.e., $K = 1$). This analysis was previously presented in Owen and Sherratt (1998) and is repeated here for completeness. For a stable steady state, we require all the roots of $P(\alpha)$ to have a negative real part. This holds if $a_1 > 0$, $a_3(1) > 0$ and $a_1a_2(1) - a_3(1) > 0$. The coefficient a_1 is strictly positive, so it remains to investigate the other two conditions. Algebraic simplification shows that these define two lines in $(\mathcal{A}, \mathcal{F})$ space which delimit the relevant regions. The condition $a_3(1) = 0$ yields

$$\mathcal{L}_1 : \mathcal{F} = k_i + \frac{d_f(k_d + k_i)}{k_a a_e} + \frac{d_f f_e k_i}{d_a a_e} - \frac{d_f f_e \mathcal{A}}{d_a a_e}, \tag{7}$$

and likewise $a_1a_2(1) - a_3(1) = 0$ gives

$$\begin{aligned} \mathcal{L}_2 : \mathcal{F} = & k_i + d_a + \frac{d_f f_e}{a_e} + \frac{d_a d_f + (d_a + d_f)(k_d + k_i)}{k_a a_e} \\ & + \frac{d_a^2(d_f + k_d + k_i) + d_a k_a(d_f f_e + d_a a_e) + k_a k_i f_e(a_1 - d_f)}{k_a a_e(a_1 - d_a)} \\ & - \frac{f_e(a_1 - d_f)\mathcal{A}}{a_e(a_1 - d_a)}. \end{aligned} \tag{8}$$

The homogeneous steady state is stable if \mathcal{F} lies below the two lines. These lines both have negative slope and are positive when $\mathcal{A} = 0$. Their relative gradients depend on the relationship between d_a and d_f , independent of the other kinetic parameters: for $d_a < d_f$, the line \mathcal{L}_1 has a more negative gradient than the line \mathcal{L}_2 ; for $d_a > d_f$, the opposite is true. Furthermore, for $d_a < d_f$ the two lines intersect at a positive value of \mathcal{F} , whereas for $d_a > d_f$ the intersection is for positive \mathcal{A} . There are thus four possible geometries for this region, according to the relative slopes of the lines and the location of their point of intersection; these are illustrated in Fig. 1.

3.2. Instability to inhomogeneous perturbations. Within the region of stability in the \mathcal{A} - \mathcal{F} plane, we now consider where the steady state is unstable for some $\lambda \neq 0$. Recall that K is a cosine function of the wavenumber λ and its range is the interval $[0, 1]$. For instability, we require that at least one root of $P(\alpha)$ is positive. Since a_1 is strictly positive, then the conditions for this are either (1) $\exists K \in [0, 1]$ such that $a_1a_2(K) - a_3(K) < 0$, or (2) $\exists K \in [0, 1]$ such that $a_3(K) < 0$. We consider these separately:

- (1) We define $\Delta(K) = a_1a_2(K) - a_3(K)$. We know that $\Delta(1) > 0$ in the region stable to homogeneous perturbations. The coefficient of K^2 in $\Delta(K)$ is negative, so that the slope of Δ must always be decreasing. Direct differentiation shows that the gradient of Δ at $K = 0$ is always negative. Thus $\Delta(K)$

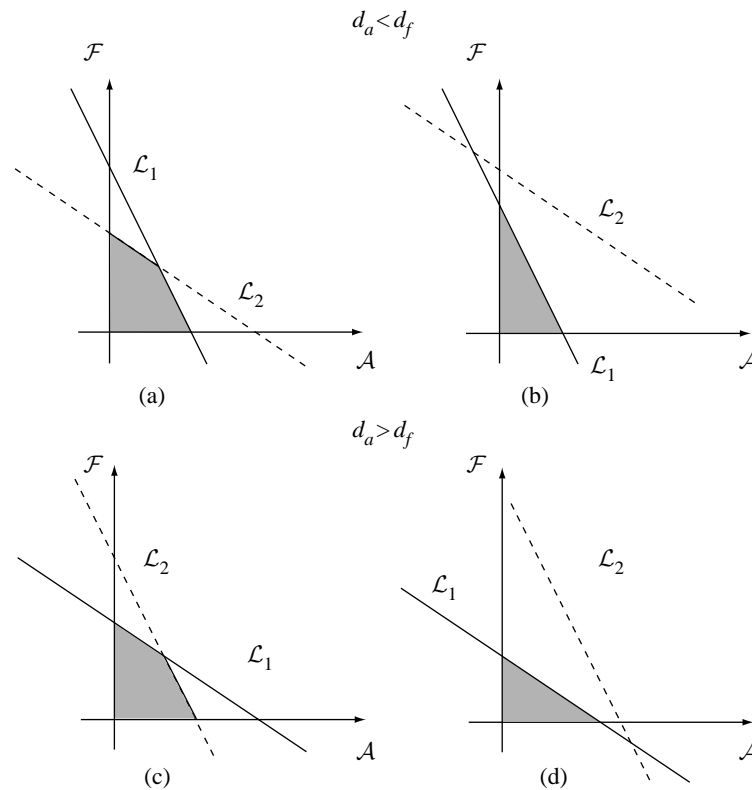


Figure 1. Schematic illustration of the possible configurations of the lines \mathcal{L}_1 (solid) and \mathcal{L}_2 (dashed). The region under both lines is such that the steady state is stable to homogeneous perturbations. Graphs (a) and (b) are the two possibilities for $d_a < d_f$, since this implies that line \mathcal{L}_1 has a more negative slope than line \mathcal{L}_2 , and that the lines must intersect at a positive value of \mathcal{F} . Similarly, cases (c) and (d) correspond to $d_a > d_f$.

must be a decreasing function on $[0, 1]$ and since it is positive at $K = 1$, it must be positive $\forall K \in [0, 1]$. This means that $\Delta(K) < 0$ is not a possible mechanism for the homogeneous steady state to become unstable to inhomogeneous perturbations.

- (2) $a_3(K)$ is also a quadratic function and as in (1) we know that $a_3(1) > 0$. However, in this case the sign of the coefficient of K^2 depends on \mathcal{F} . Thus there are two sub-cases to consider: (a) when the coefficient of K^2 is negative and (b) when the coefficient is positive. In the following analysis we will use the fact that the critical point of $a_3(K)$ is at:

$$K_{\text{crit}} = \frac{d_f \mathcal{A}}{2k_a a_e \left(\mathcal{F} - k_i - \frac{k_d d_f}{k_a a_e} \right)}. \quad (9)$$

- (a) First we consider the case when the coefficient of K^2 in a_3 is negative, i.e., when $\mathcal{F} < k_i + \frac{k_d d_f}{k_a a_e}$. Then $a_3(K)$ is a decreasing function on

$[0, 1]$ and by the same argument as in (1), $a_3(K)$ is strictly positive $\forall K \in [0, 1]$. Thus for these values of \mathcal{F} the steady state is stable to inhomogeneous perturbations.

- (b) We now assume that the coefficient of K^2 is positive; we consider those values of $\mathcal{F} > k_i + \frac{k_d d_f}{k_a a_e}$. Therefore K_{crit} is positive and corresponds to a minimum. This case then subdivides into whether (i) $K_{\text{crit}} > 1$ or (ii) $K_{\text{crit}} \in [0, 1]$; these are separated in the \mathcal{A} - \mathcal{F} plane by the line

$$\mathcal{L}_3 : \mathcal{F} = k_i + \frac{k_d d_f}{k_a a_e} + \frac{d_f}{2k_a a_e} \mathcal{A}. \quad (10)$$

- (i) Consider $K_{\text{crit}} > 1$. Since the slope of $a_3(K)$ is always increasing and is zero at $K_{\text{crit}} > 1$, $a_3(K)$ must have negative slope over the interval $[0, 1]$. But $a_3(1) > 0$, so $a_3(K)$ must be positive $\forall K \in [0, 1]$. Therefore $K_{\text{crit}} > 1$ does not give conditions for pattern formation.
- (ii) Now consider $K_{\text{crit}} \in [0, 1]$. This holds if \mathcal{F} lies above the line \mathcal{L}_3 . In order for $a_3(K)$ to be negative for some K its minimum value, $a_3(K_{\text{crit}})$, must be less than zero. We therefore look for the bifurcation when $a_3(K_{\text{crit}})$ is equal to zero. This occurs on the following curve

$$\mathcal{C} : \mathcal{F} = k_i + \frac{d_f(2k_d + k_i)}{2k_a a_e} \pm \frac{d_f}{2k_a a_e} \sqrt{k_i^2 - \frac{k_a f_e \mathcal{A}^2}{k_a f_e + d_a}}. \quad (11)$$

The minimum value is less than zero when \mathcal{F} lies outside the interval between the two values defined in (11). However, we have already assumed that \mathcal{F} lies above the line \mathcal{L}_3 given in (10). Straightforward algebra shows that \mathcal{L}_3 intersects the curve \mathcal{C} at $\mathcal{A} = 0$ and at its point of intersection with \mathcal{L}_1 . This means that only those \mathcal{F} greater than the largest of the two values defined in (11) are relevant for pattern formation.

In summary, we have three conditions that delimit the region in $(\mathcal{A}, \mathcal{F})$ space where patterns may form:

$$\begin{aligned} \mathcal{F} &< k_i + \frac{d_f(k_d + k_i)}{k_a a_e} + \frac{d_f f_e k_i}{d_a a_e} - \frac{d_f f_e \mathcal{A}}{d_a a_e} & (12a) \\ \mathcal{F} &< k_i + d_a + \frac{d_f f_e}{a_e} + \frac{d_a d_f + (d_a + d_f)(k_d + k_i)}{k_a a_e} \\ &+ \frac{d_a^2(d_f + k_d + k_i) + d_a k_a(d_f f_e + d_a a_e) + k_a k_i f_e(a_1 - d_f)}{k_a a_e(a_1 - d_a)} \end{aligned}$$

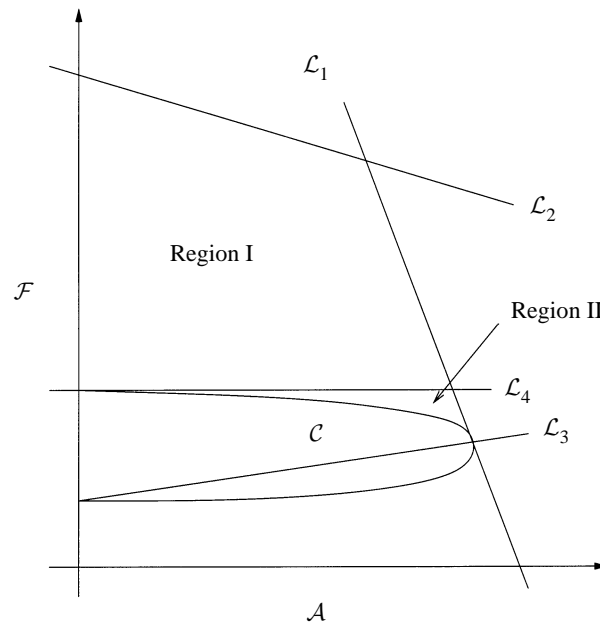


Figure 2. Qualitative illustration of the parameter space in the \mathcal{A} - \mathcal{F} plane where pattern formation is possible. Below the lines \mathcal{L}_1 and \mathcal{L}_2 , the homogeneous equilibrium is stable to homogeneous perturbations; this is configuration (a) of Fig. 1. Above the curve \mathcal{C} , the steady state is also unstable to inhomogeneous perturbations. The region for pattern formation is therefore defined by the \mathcal{F} -axis, the lines \mathcal{L}_1 and \mathcal{L}_2 , and the curve \mathcal{C} . For mathematical convenience, we divide this region into two parts by the line \mathcal{L}_4 , defined in equation (14).

$$\frac{f_e(a_1 - d_f)\mathcal{A}}{a_e(a_1 - d_a)} \quad (12b)$$

$$\mathcal{F} > k_i + \frac{d_f(2k_d + k_i)}{2k_a a_e} + \frac{d_f}{2k_a a_e} \sqrt{k_i^2 - \frac{k_a f_e \mathcal{A}^2}{k_a f_e + d_a}}. \quad (12c)$$

A qualitative illustration of these conditions is given in Fig. 2. In particular, it is clear that patterns are possible for zero ligand feedback ($\mathcal{A} = 0$), but not zero receptor feedback. As we discuss below, the region of pattern formation divides naturally into two parts.

3.3. Range of unstable wavenumbers. When \mathcal{A} and \mathcal{F} lie in the region defined by (12a)–(c), the range of unstable wavenumbers, λ , satisfies the inequality $a_3(K(\lambda)) < 0$. To admit the possibility of a pattern-generating mechanism, the coefficient of the quadratic term of a_3 must be positive. Thus, the range of unstable λ are those lying between the two roots of $a_3 = 0$. Solving this equation for K

gives the following expression for the roots of a_3 :

$$K_{\pm} = K_{\text{crit}} \pm \frac{\sqrt{(d_f \mathcal{A})^2 + (2k_a a_e)^2 \left(1 + \frac{d_a}{k_a f_e}\right) \left(\mathcal{F} - k_i - \frac{k_d d_f}{k_a a_e}\right) \left(\mathcal{F} - k_i - \frac{d_f(k_d + k_i)}{k_a a_e}\right)}}{2k_a a_e \left(\mathcal{F} - k_i - \frac{k_d d_f}{k_a a_e}\right)} \quad (13)$$

where K_{crit} is defined above in equation (9).

To further investigate those wavenumbers that we would expect to see in the solution of the full set of nonlinear equations, we wish to find the K corresponding to the fastest growing mode; this is the pattern that we expect to dominate. Firstly, we look in more detail at the form of the dispersion relation $P(\alpha) = \alpha^3 + a_1 \alpha^2 + a_2(K)\alpha + a_3(K) = 0$ to show that there is only one possible positive real root and estimate the K which gives the largest value of this root; recall that α is the growth rate of perturbations with wavenumber λ .

For the parameter regime where patterns may develop, we already know that $a_1 > 0$ and $a_3(K) < 0$. It remains to consider the form of the coefficient of α , $a_2(K)$, for $K \in [0, 1]$; $a_2(K)$ is defined in (6b). The coefficient of K^2 is negative, so that the slope of $a_2(K)$ is always decreasing, with the maximum value of $a_2(K)$ at $K = -\mathcal{A}/2(k_a a_e + k_d) < 0$. Moreover, $a_1 a_2(1) > a_3(1) > 0$, where $a_1 > 0$, so that $a_2(1) > 0$. Therefore $a_2(K) > 0$ for all $K \in [0, 1]$. Thus, the coefficients of α^2 and α are both positive for the whole range of K , and so $P(\alpha)$ is strictly increasing for $\alpha > 0$. Since $P(0) = a_3(K) < 0$, $P(\alpha)$ must have a unique positive real root, α^* say, which increases as the magnitude of $a_3(K)$ increases. The exact way in which this occurs also depends on $a_2(K)$: if we consider $P(\alpha)$ for small α and neglect the nonlinear terms, $\alpha^* \approx -a_3(K)/a_2(K)$. However, it is reasonable to suggest that a good approximation of the K corresponding to the largest possible α^* is given by K_{crit} , since K_{crit} maximizes $-a_3(K) \forall K \in [0, 1]$. Moreover, we expect K_{crit} to be an underestimate, rather than an overestimate, for the value of K at which the growth rate α^* attains its maximum, since $a_2(K)$ is a decreasing function on the interval $[0, 1]$ and so for $K < K_{\text{crit}}$, $-a_3(K)/a_2(K) < -a_3(K_{\text{crit}})/a_2(K_{\text{crit}})$. Numerical simulation of the dispersion relation in Fig. 3 illustrates this and shows that the value of K giving the maximum α^* is just above K_{crit} .

We will now look at how K_{crit} and the range of unstable K vary in different areas of the parameter region. For convenience we divide the region into two parts using the line

$$\mathcal{L}_4 : \mathcal{F} = k_i + \frac{d_f(k_d + k_i)}{k_a a_e} \quad (14)$$

which intersects the curve \mathcal{C} at $\mathcal{A} = 0$ and the line \mathcal{L}_1 at $\mathcal{A} = k_i$. We refer to the region of the \mathcal{A} - \mathcal{F} plane above this line as region I, with region II below the line, as illustrated in Fig. 2. The motivation for this division is that along the line \mathcal{L}_4 , the smallest root of $a_3(K)$, K_- defined in (13), is zero. If $K_- < 0$, as is the case for values of \mathcal{F} above \mathcal{L}_4 , then the minimum unstable K is always zero, since

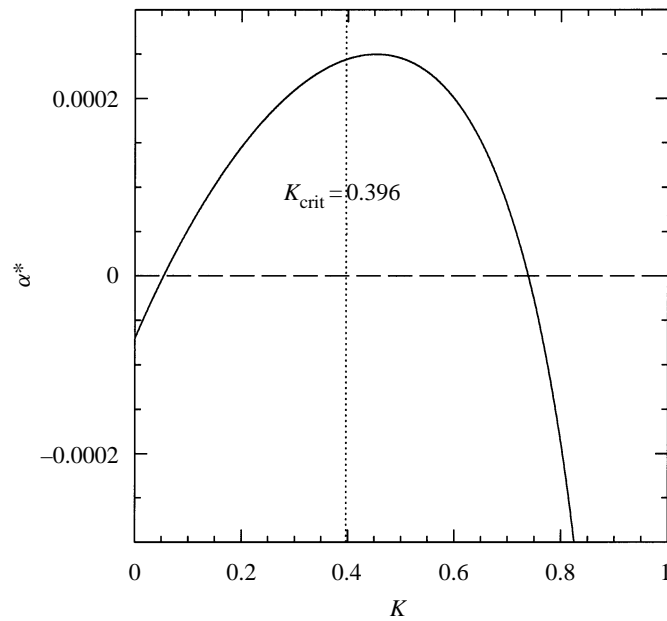


Figure 3. Dispersion relation plotting α^* , the largest root of $P(\alpha) = 0$, for the whole range of K . Those values of K for which $\alpha^* > 0$ and perturbations grow satisfy the inequality $a_3(K) < 0$. The dotted vertical line denotes K_{crit} , which is just below the value of K that corresponds to the maximum value of α^* , the fastest growing mode. This suggests that K_{crit} gives a good indication of the pattern mode that we expect to dominate. The values of the free parameters in the feedback functions are $C_2 = 8000$, $m = 1$, $n = 3$. The other parameters are $k_a = 0.0003 \text{ molecule}^{-1} \text{ min}^{-1}$, $k_d = 0.12 \text{ min}^{-1}$, $k_i = 0.019 \text{ min}^{-1}$, $d_a = 0.006 \text{ min}^{-1}$, $d_f = 0.03 \text{ min}^{-1}$, $f_e = 3000$, $b_e = 3000$, $r_0 = 3000$, $r_m = 25500$.

$K \in [0, 1]$. Consequently, in region I the range of unstable K is $[0, K_+]$, whereas in region II the range is $[K_-, K_+]$.

Before considering each region in turn, we need to discuss the relationship between the function K and the wavelength (in terms of the number of cells)

$$\omega = \frac{2\pi}{\lambda} = \frac{2\pi}{\cos^{-1}(2K - 1)}. \quad (15)$$

Since our system is spatially discrete, we are only concerned with integer values of the wavelength ω that correspond to a periodic pattern of ligand molecules and free and bound receptors on the cell surface; i.e., those ω with integer parts ≥ 2 . Thus, we need only consider $\lambda \in [0, \pi]$, and therefore for all unstable $K \in [0, 1]$ there exists a unique wavelength, $\omega \geq 2$. Figure 4 illustrates the relationship between ω and K for $\lambda \in [0, \pi]$.

For ease of notation in the following discussion, we need to define those wavelengths which correspond to the lower and upper limits of the unstable K and to K_{crit} (an approximation of the fastest growing mode). Recall that K_{\pm} are the roots of $a_3(K)$ defined in equation (13), and so the lower limit of the unstable K is de-

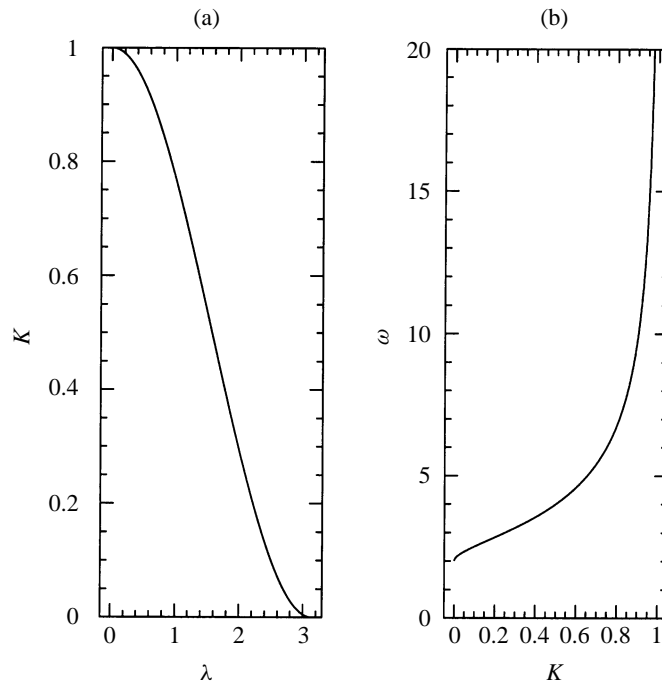


Figure 4. Graphs illustrating: (a) K as a function of λ for $\lambda \in [0, \pi]$; and (b) the relationship between the wavelength ω and K , where ω is defined in equation (15). This shows that for all unstable $K \in [0, 1]$ there is a unique value of $\omega \geq 2$, which are the values of interest for fine-grained cellular patterns.

defined as $\max(0, K_-)$, while the upper limit is given by K_+ . We therefore denote ω_- as 1 plus the integer part of the minimum unstable wavelength, i.e., the wavelength corresponding to the minimum unstable K . Similarly, ω_+ denotes the integer part of the maximum unstable wavelength. Finally, we define ω_{crit} to be the nearest integer to the wavelength when $K = K_{\text{crit}}$. We note that the term ‘single-mode pattern’ will be used to describe a pattern where only a single wavelength is unstable.

3.3.1. *Region I.* We first consider possible patterning modes in region I, defined as the area below the lines \mathcal{L}_1 and \mathcal{L}_2 and bounded by the \mathcal{F} -axis and the line \mathcal{L}_4 , see Fig. 2. The key properties are as follows:

- A wavelength of two cells is always unstable. The range of unstable K is between 0 and K_+ , since K_- is strictly negative for \mathcal{F} above the line \mathcal{L}_4 . This means that a pattern with wavelength two is possible for all $(\mathcal{A}, \mathcal{F})$ in this region. Consequently, single-mode patterns with wavelength greater than two are not predicted in region I.
- There is no upper bound on the unstable wavelengths. Figure 5 shows the range of possible wavelengths in different parts of region I for specified parameter values. The region is divided according to the value of ω_+ for each

$(\mathcal{A}, \mathcal{F})$. The range of unstable ω is extended as both \mathcal{A} and \mathcal{F} increase; in particular, those values where only a wavelength of 2 is predicted are close to $\mathcal{A} = 0$ and the line \mathcal{L}_4 . As $(\mathcal{A}, \mathcal{F})$ approaches the line \mathcal{L}_1 , it appears from numerical calculations that ω_+ is unbounded. Indeed, if we substitute the equation for \mathcal{L}_1 , (7), into the equation for K_+ , (13), algebraic manipulation gives $K_+ = 1$; equivalent to $\omega_+ \rightarrow \infty$. Thus, close to the line \mathcal{L}_1 , ω_+ is unbounded, which implies that there are parameter sets in region I where a pattern of any wavelength is possible. However, if we now consider how K_{crit} varies, these patterns of arbitrarily long wavelength are not those we would expect to see.

- The wavelength of the fastest growing mode is bounded. Along the line \mathcal{L}_4 , $K_{\text{crit}} = \frac{\mathcal{A}}{2k_i}$ where $\mathcal{A} \in [0, k_i]$. Above this line, $0 \leq K_{\text{crit}} < \frac{\mathcal{A}}{2k_i}$. Therefore, in region I, $K_{\text{crit}} \in [0, \frac{1}{2})$, i.e., $\omega_{\text{crit}} \in [2, 4)$. This bound on ω_{crit} in region I means that we would expect wavelengths of 2 or 3 cells to dominate the pattern form.

3.3.2. *Region II.* Region II is the region of parameter space between the line \mathcal{L}_4 and the curve \mathcal{C} , bounded by \mathcal{L}_1 (in the case $d_a < d_f$). We analyse the unstable pattern modes below:

- Single-mode patterns with a wavelength greater than 2 are possible close to the curve \mathcal{C} . The range of unstable K is now between K_- and K_+ , since K_- takes positive values in region II. Therefore $\omega_- > 2$ for all $(\mathcal{A}, \mathcal{F})$ in this region. Along the curve \mathcal{C} , the roots of $a_3(K)$ both equal K_{crit} . Thus, as \mathcal{C} is approached, the only possible wavelength is that corresponding to K_{crit} , where

$$K_{\text{crit}} = \frac{\mathcal{A}}{k_i + \sqrt{k_i^2 - \frac{k_a f_e \mathcal{A}^2}{k_a f_e + d_a}}}. \quad (16)$$

- There is no upper bound on the unstable wavelengths. Figure 6 illustrates the minimum and maximum values of the range of unstable wavelengths for region II, as well as those $(\mathcal{A}, \mathcal{F})$ where only one pattern mode is predicted by linear analysis. K_- is equal to zero along the line \mathcal{L}_4 , but varies from 0 to 1 along the curve \mathcal{C} and the line \mathcal{L}_1 . Thus the corresponding wavelength, ω_- , increases as \mathcal{F} decreases as shown in Fig. 6(a). From region I, we know that $K_+ = 1$ along \mathcal{L}_1 ; K_+ also varies between 0 and 1 along both \mathcal{L}_4 and \mathcal{C} . Thus the maximum unstable wavelength increases without bound with both \mathcal{A} and \mathcal{F} , as shown in Fig. 6(b). Finally, the single-mode patterns form a small region close to the curve \mathcal{C} , as is expected since $\omega_{\pm} = \omega_{\text{crit}}$ along \mathcal{C} .
- The wavelength of the fastest growing mode is unbounded. We now look at how K_{crit} varies in region II. \mathcal{A} takes values between 0 and \mathcal{A}_{max} where

$$\mathcal{A}_{\text{max}} = \frac{2k_i(k_a f_e + d_a)}{2k_a f_e + d_a} \quad (17)$$

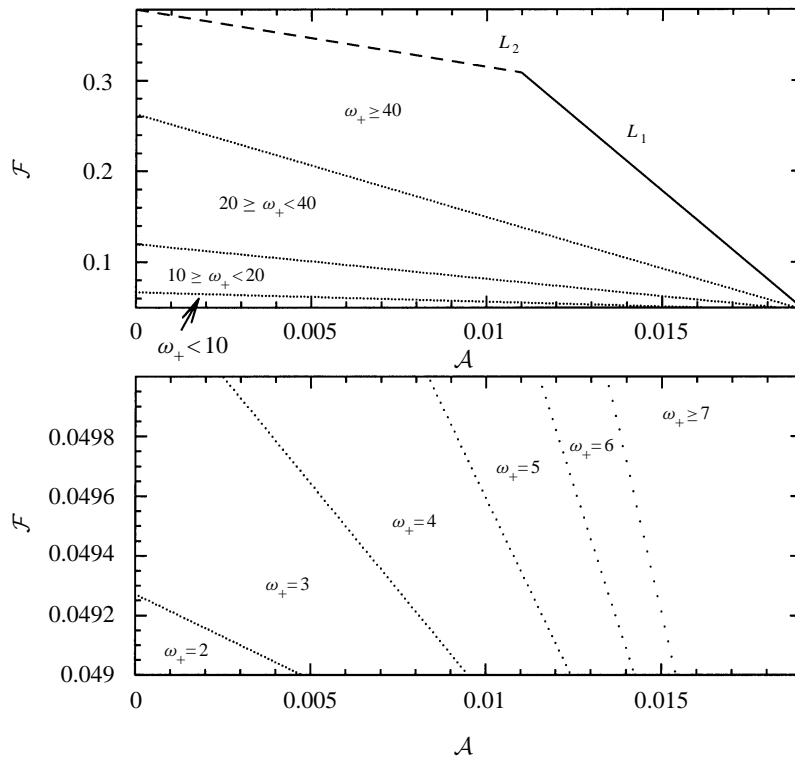


Figure 5. Contours of the maximum unstable wavelength in region I. The region is delimited by the \mathcal{F} -axis and the lines \mathcal{L}_1 (solid), \mathcal{L}_2 (dashed) and \mathcal{L}_4 ($\mathcal{F} = 0.049$). Together these two graphics represent region I of the parameter regime. The lower diagram is to a larger \mathcal{F} scale to give a clearer picture of the changes in wavelength near to the line \mathcal{L}_4 . The minimum value of the range of unstable wavelengths is always 2; the region is divided according to the integer part of the upper limit, denoted by ω_+ . Observe that the range of unstable ω extends as both \mathcal{A} and \mathcal{F} increase. In particular, those values where only a wavelength of 2 is predicted are close to $\mathcal{A} = 0$ and the line \mathcal{L}_4 . Parameter values used in the calculations are as in Fig. 3.

is the value of \mathcal{A} at which \mathcal{C} intersects \mathcal{L}_1 . Substituting \mathcal{A}_{\max} into the equation for K_{crit} along \mathcal{C} (16) gives $K_{\text{crit}} = 1$. Therefore K_{crit} varies over the whole interval $[0, 1]$, as \mathcal{A} is varied along the curve \mathcal{C} . This corresponds to $\omega_{\text{crit}} \in [2, \infty)$, and so in contrast to region I, the wavelength of the pattern that we expect to dominate has no upper bound for certain $(\mathcal{A}, \mathcal{F})$ in region II. Although this implies that we would expect to see patterns of any wavelength, that part of the parameter regime where longer wavelengths are unstable is very small.

In summary, single-mode patterns with a wavelength greater than 2 are only possible in region II; and in theory there is no bound on the unstable wavelength for parts of the parameter space. Multi-mode patterns are possible in both regions,

with no upper bound for the wavelength in either region; a pattern of wavelength 2 is always unstable in region I. The wavelength corresponding to the fastest growing mode, ω_{crit} , takes the values 2 or 3 in region I with no such bound in region II.

4. NUMERICAL SIMULATION OF THE MODEL

In this section we present the results of numerical simulations testing the predictions of our linear analysis. We begin by briefly discussing the choice of parameter values and the particular form of the feedback functions.

The parameter values used in the model simulation are for the particular case of TGF α binding to EGF-R. An explanation of the choice of each individual value can be found in the work of Owen and Sherratt (1998). In particular, they based kinetic parameters on the data of Waters *et al.* (1990) for EGF binding to EGF-R. Following this approach, we fix all parameters not associated with the feedback functions; these values are listed in the legend of Fig. 3. Specifying the forms of the feedback functions, P_a and P_f , is more difficult since the data available on production rates of ligand and receptors is extremely limited. However, this can be achieved to some extent because the functions must satisfy a number of conditions that relate them to experimentally measurable quantities:

- (i) In the absence of any ligand binding at the cell surface, there will be a background level of receptor expression, say r_0 . This is a homogeneous steady state of the model, and so the equation for f (1b) gives

$$P_f(0) = d_f r_0. \quad (18)$$

- (ii) Specifying the equilibrium levels of free and bound receptors, f_e and b_e , defines the steady state level of free ligand, a_e , implicitly through equation (1c) as well as the values of the feedback functions at the steady state, so that

$$a_e = \frac{b_e(k_d + k_i)}{k_a f_e}, \quad P_a(b_e) = k_i b_e + d_a a_e, \\ \text{and} \quad P_f(b_e) = k_i b_e + d_f f_e. \quad (19)$$

- (iii) There will also be a maximum possible level of receptor expression, r_m , say. This can be estimated experimentally by saturating cells with ligand. Such saturation means that the rate of internalization of bound receptors must be equal to the rate of free receptor production, giving

$$P_f(r_m) = k_i r_m. \quad (20)$$

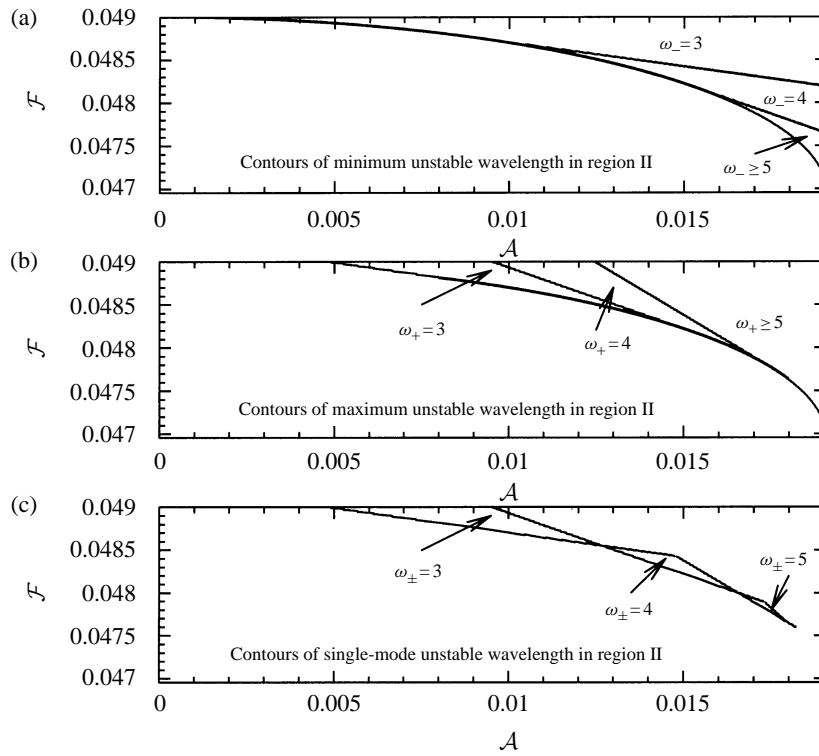


Figure 6. Contours of the minimum and maximum unstable wavelengths, and the values of \mathcal{A} and \mathcal{F} where a single pattern mode is unstable in region II. The region is delimited by the curve \mathcal{C} and the lines \mathcal{L}_1 (on this scale the right-hand axis) and \mathcal{L}_4 ($\mathcal{F} = 0.049$). Graphs (a) and (b) show the lower and upper limits of the range of unstable wavelengths for region II; ω_- denotes 1 plus the integer part of the minimum unstable wavelength, while ω_+ denotes the integer part of the maximum unstable wavelength, as in Fig. 5. The minimum ω increases as \mathcal{F} decreases, whereas the maximum ω increases as \mathcal{A} and \mathcal{F} increase. Graph (c) illustrates that, as expected, the single-mode patterns are close to the curve \mathcal{C} ; on this scale we can see where patterns of 3, 4 and 5 cells are predicted. Parameter values used in the calculations are as in Fig. 3.

In our numerical simulations, we will consider feedback functions of Hill form:

$$P_a(b) = \frac{C_1^m b^m}{C_2^m + b^m} \quad (21a)$$

$$P_f(b) = C_3 + \frac{C_4^n b^n}{C_5^n + b^n}. \quad (21b)$$

The parameters C_1 , C_3 , C_4 and C_5 are constrained by conditions (18)–(20), leaving three free parameters, C_2 , m and n , which can be varied in model simulations. Our objective is to confirm the types of pattern predicted by linear analysis, where we took \mathcal{A} and \mathcal{F} to be controlling parameters. It is therefore necessary to consider how we can vary \mathcal{A} and \mathcal{F} using the free parameters of the model. By fixing C_2 , m can be used to vary \mathcal{A} and n to vary \mathcal{F} . If we increase C_2 , a smaller range of m is required to vary \mathcal{A} over the parameter space.

We solve the nonlinear ordinary differential equations (1a)–(c) numerically using a fourth- and fifth-order Runge–Kutta method. To simulate cells as part of a continuum, we take our boundary conditions to be periodic. The initial conditions are small random perturbations about the homogeneous steady state, within $\pm 1\%$ of the equilibrium.

Before we study the numerical results in detail, we begin by noting that all the simulations we carried out agree with the analysis concerning when patterns form. The differences between the predictions of the linear analysis and the numerical solution of the nonlinear differential equations occur in the pattern wavelengths, as we shall discuss using the results below.

4.1. Numerical solutions on an array of 30 cells. Firstly, we describe simulations on an array of 30 cells. We would expect to be able to see patterns with wavelengths of 2, 3, 5, 6, etc. cells, since these are all divisors of 30. Linear analysis predicts that for a few values of \mathcal{A} and \mathcal{F} in region I, the unstable K correspond to a single wavelength of 2 cells. We solve the model for such parameter values; the results of the simulations are illustrated in Fig. 7. None of the solutions for this set of parameters form a regular pattern, and those that almost develop to a single-mode pattern tend towards a wavelength of 4 cells. To examine this phenomenon more closely, we investigate the temporal evolution of the pattern. We therefore look at a solution of the model for just one of the variables in more detail, at six time intervals (Fig. 8). We use different parameter values for which the uniform steady state is more unstable to random perturbations and so the pattern evolves much quicker than in Fig. 7. Nevertheless, the behaviour remains the same. We observe that the formation of the pattern appears to occur once distinct peaks in the number of free receptors are established. These peaks then grow to the detriment of the number of free receptors in neighbouring cells; high numbers of receptors are never found in consecutive cells. It also seems that the distance between the development of the first peaks determines whether other peaks can evolve between

them, and if so, with what frequency. We notice from Fig. 7 that, over the array of 30 cells, a peak in the number of free receptors corresponds to both a peak in the number of bound receptors and a trough in the number of ligand molecules.

Intuitively, we can explain this by considering the situation of a particular cell, j say, where a peak in the number of occupied receptors has formed. The increase in bound receptors up-regulates production of both ligand molecules and free receptors, although this is more pronounced for free receptors since receptor feedback is stronger than ligand feedback (i.e., $\mathcal{F} > \mathcal{A}$). This balance in feedback strengths will be discussed later. The number of ligand molecules decreases due to a combination of weaker ligand feedback and our assumption that the cells are part of a regular two-dimensional grid; so that there is always an excess of free receptors on two identical neighbouring cells to bind to ligand in cell j , keeping the level of ligand low. Once established, the peaks in free and occupied receptors in cell j grow, while those in neighbouring cells, $j - 1$ and $j + 1$, decrease. This can be explained by the competition to bind to ligand molecules in cell j : those cells with fewer free receptors will bind to less ligand and form fewer bound receptor complexes. The number of occupied receptors on the surface of cells $j - 1$ and $j + 1$ therefore decreases, and consequently reduces their production of free receptors. The relative size and position of initial peaks in bound receptors thus dictates the subsequent development of the pattern.

The differences between the linear analysis and the numerical solutions for parameters in region I prompted us to test the analysis by solving the linearized equations (3a)–(c) numerically. For different parameter sets, the pattern wavelength observed in each case was in agreement with the linear analysis. Therefore, we can only conclude that the nonlinearities in the model override the wavelengths predicted by the linearized system.

For parameters in region II, single-mode patterns of a range of wavelengths are predicted by linear analysis and this is confirmed in numerical simulations. Moreover, the separation of the peaks depends crucially on the feedback strengths; numerical investigation demonstrates that increasing the strength of ligand production induces longer range patterns. Figure 9 shows the results of simulations in which the strength of receptor up-regulation (\mathcal{F}) is kept fixed while the strength of ligand feedback (\mathcal{A}) is allowed to vary. In these simulations, we observe patterns with wavelengths of between 5 and 15 cells as ligand feedback is increased. The outcome of these numerical studies agrees qualitatively with our analytical predictions for ω_{crit} , the wavelength that we expect to dominate in the solution of the model. If the strength of receptor feedback is also increased, then numerical results (not shown) indicate that the average wavelength decreases. Therefore, the longer range wavelengths are generated by the strongest feedback in ligand production and the weakest feedback in receptor production that still enable patterns to evolve.

4.2. Numerical solutions on an array of 60 cells. By doubling the number of cells in the model, regular patterns of wavelength 4 are now a possible solution

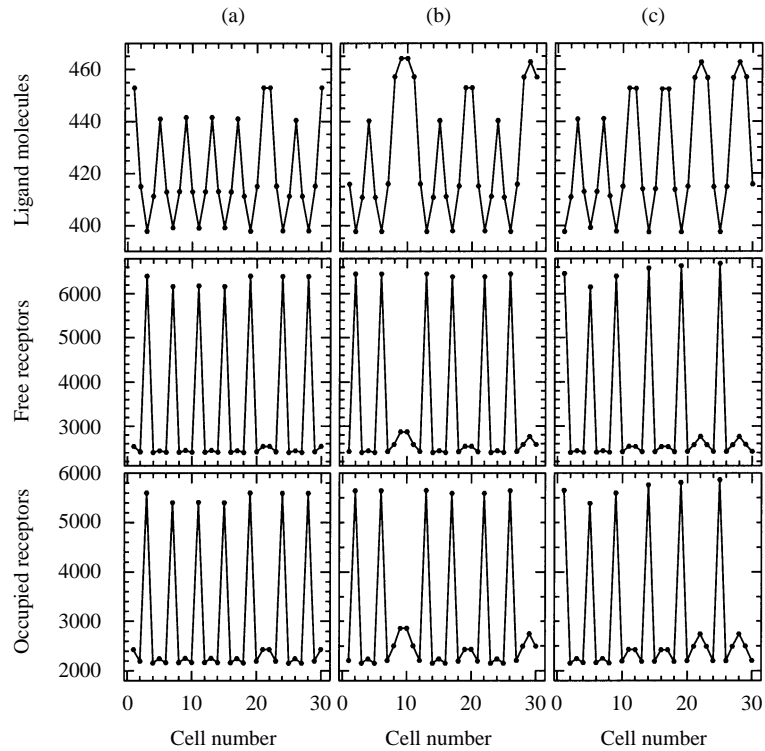


Figure 7. Three solutions of the model for 30 cells, each corresponding to different (random) initial conditions. Linear analysis predicts the formation of a pattern with a wavelength of 2 cells. In all the simulations of the nonlinear equations for these parameter values we observe no regular form of pattern. The nearest solution to a pattern with a wavelength of four cells is illustrated in (a); a regular pattern of mode 4 is not possible in this case since 4 is not a divisor of 30. Notice that peaks in the number of free and bound receptors, which are always at least four cells apart, correspond to troughs in the number of ligand molecules. Intuitively, we can explain this by considering the situation of a particular cell, j say, where a peak in the number of occupied receptors has formed. Production of ligand molecules and free receptors is up-regulated by bound receptors until the point of saturation; hence the high number of free receptors. However, the number of ligand molecules decreases due to our assumption that the cells are part of a regular two-dimensional grid; so that the high number of free receptors in two identical neighbouring cells bind to the ligand molecules in cell j . The values of the free parameters in the feedback functions are $C_2 = 2500$, $m = 0.1013$ and $n = 3.1059$. The other parameters are as in Fig. 3. The profiles are for $t = 1800$ h.

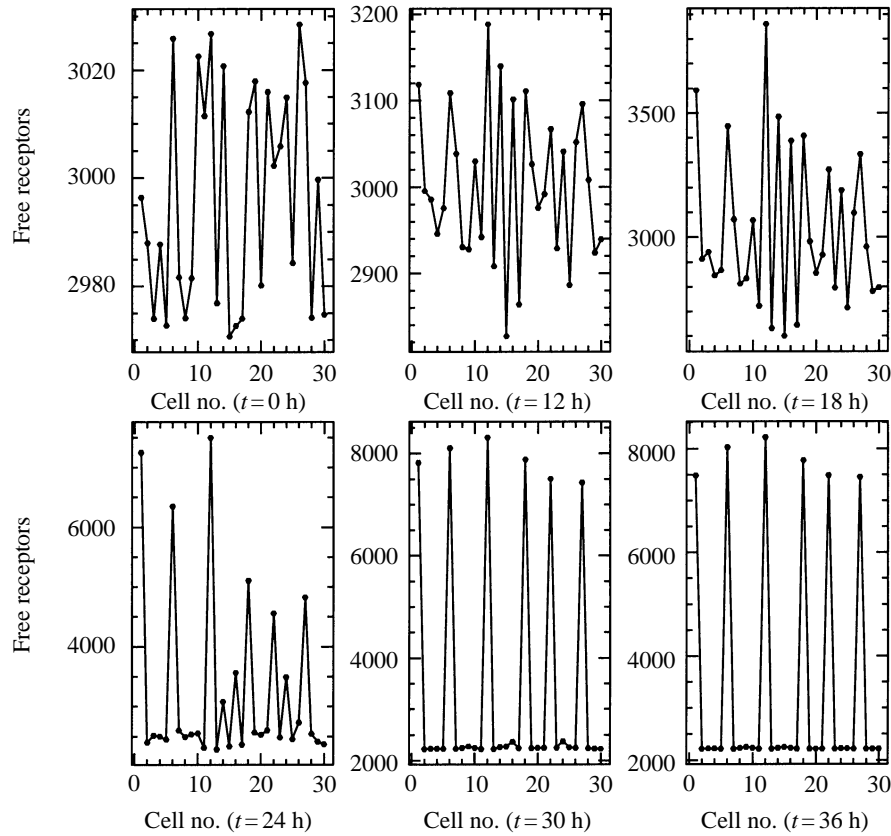


Figure 8. Temporal evolution of the free receptor profile in a solution of the nonlinear model. Between 18 and 24 hours, several distinct peaks appear. Once established, these peaks grow to the detriment of the number of free receptors in neighbouring cells. This can be explained by the ‘competition’ to bind to ligand molecules in cells with such high numbers of receptors. From Fig. 7 we can see that cells where these peaks occur have the smallest numbers of ligand molecules, and so free receptors in neighbouring cells have fewer ligands to bind to. Therefore the number of occupied receptors on the surface of neighbouring cells decreases, which reduces their production of free receptors. The distance between the early peaks appears to determine whether other peaks will consequently form between them, and if so, with what frequency. The values of the free parameters in the feedback functions are $C_2 = 2500$, $m = 1$ and $n = 3.5$. Time t is given in hours. The other parameters are as in Fig. 3.

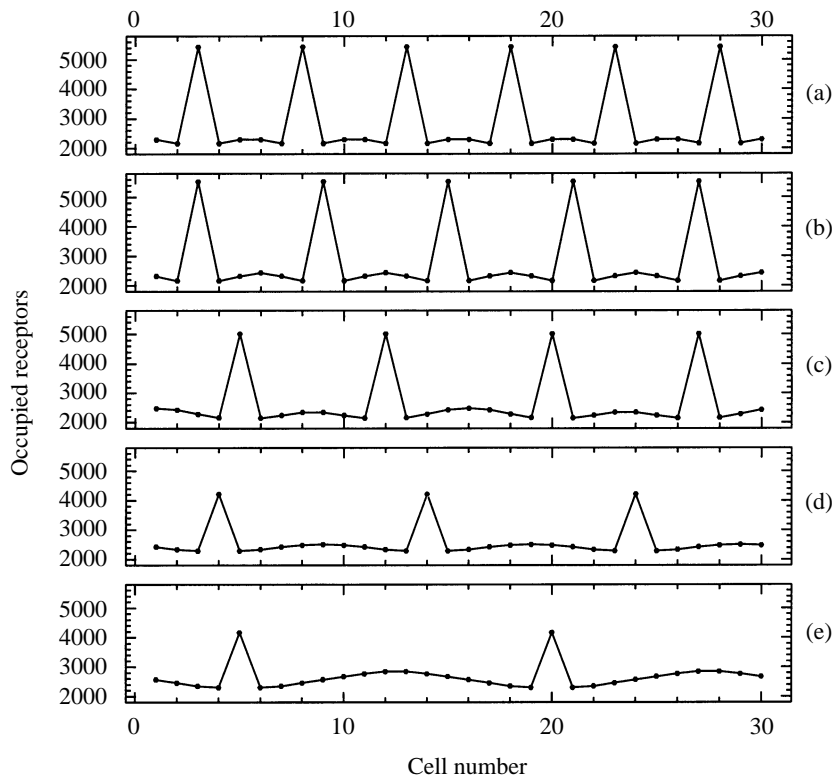


Figure 9. The bound receptor profile for five different simulations of the model. Longer range patterns are generated by increased ligand feedback: the distance between the peaks in occupied receptors increases as the strength of the ligand production increases, the weakest feedback being in (a) and the strongest in (e). This agrees qualitatively with the predictions of the linear analysis for the wavelength that we expect to dominate in the solution of the full model. The values of the free parameters in the feedback functions are $C_2 = 2500$, $n = 3$ and m varies in each simulation as follows: (a) 0.8, (b) 1.0, (c) 1.5, (d) 1.87 (e) 1.95. As m increases, the strength of ligand up-regulation, \mathcal{A} , increases. The other parameters are as in Fig. 3. Time $t = 1800$ h.

form. We start by looking at simulations for those parameters in region I where linear analysis predicted pattern formation with a wavelength of 2 cells. This is the situation illustrated in Fig. 7 for 30 cells. Figure 10 shows that, as in the case of 30 cells, we do not observe a regular form of pattern in the solution of the nonlinear model: as the initial conditions vary, the pattern form changes. To check that a pattern of mode 2 was unstable for these parameters, we used as our initial conditions, perturbations of wavelength equal to 2 cell lengths about the homogeneous steady state, and observed the solution over time. The pattern did not decay and so we conclude that the linear analysis is correct in predicting that a wavelength of two cells is unstable for these parameter values.

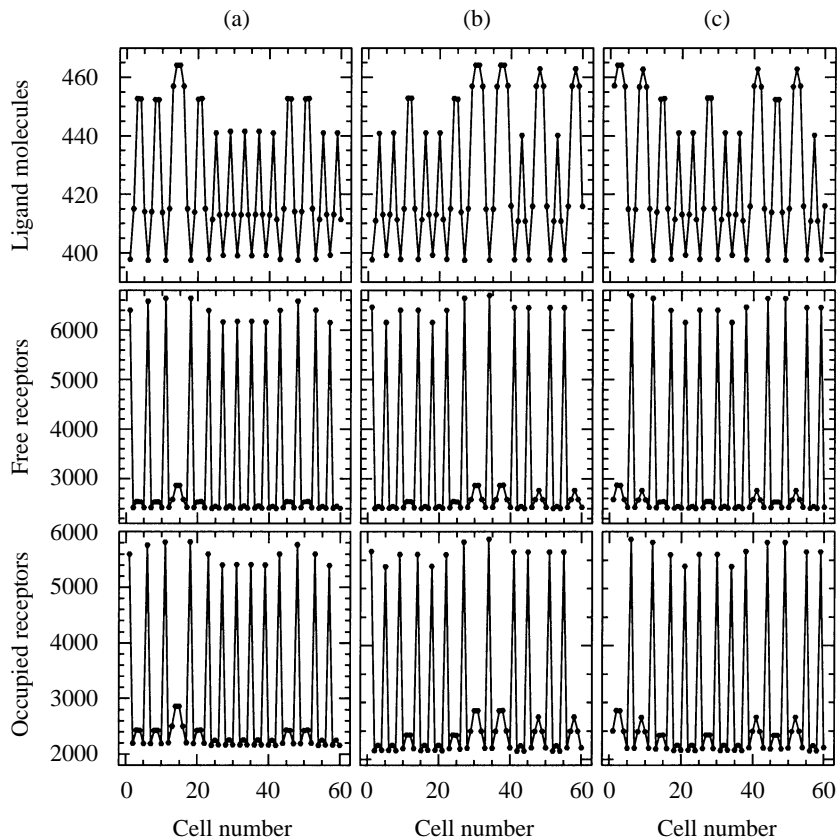


Figure 10. Three solutions, (a), (b), (c) of the model for 60 cells, each corresponding to different (random) initial conditions. The parameter values are the same in all three cases, as given in Fig. 7. Linear analysis predicts the formation of a pattern with a wavelength of 2 cells. In all the simulations of the nonlinear equations for these parameter values we observe no regular form of pattern. Time $t = 3600$ h.

4.3. Multi-mode solutions. The parameter values used in the above simulations were all for regions where linear analysis predicts a single unstable wavelength. We now consider some parameter regions where linear analysis predicts a range of unstable wavelengths. Solution of the nonlinear equations for parameter values in region I where wavelengths 2, 3 and 4 are predicted to be unstable by linear analysis results in no regular form of pattern (not shown). However, the peaks in the number of free and bound receptors are at similar levels to those in solutions with previous parameter sets. Figure 11 illustrates simulations for values of \mathcal{A} and \mathcal{F} in region I where the unstable wavelengths ω range from 2 to 56. The ω_{crit} corresponding to K_{crit} —an approximation of the fastest growing mode—is 2. The solution is quite different from previous simulations: again there is no regular form of pattern, but here we see many more peaks in the number of receptors, and much lower levels of ligand molecules and occupied receptors.

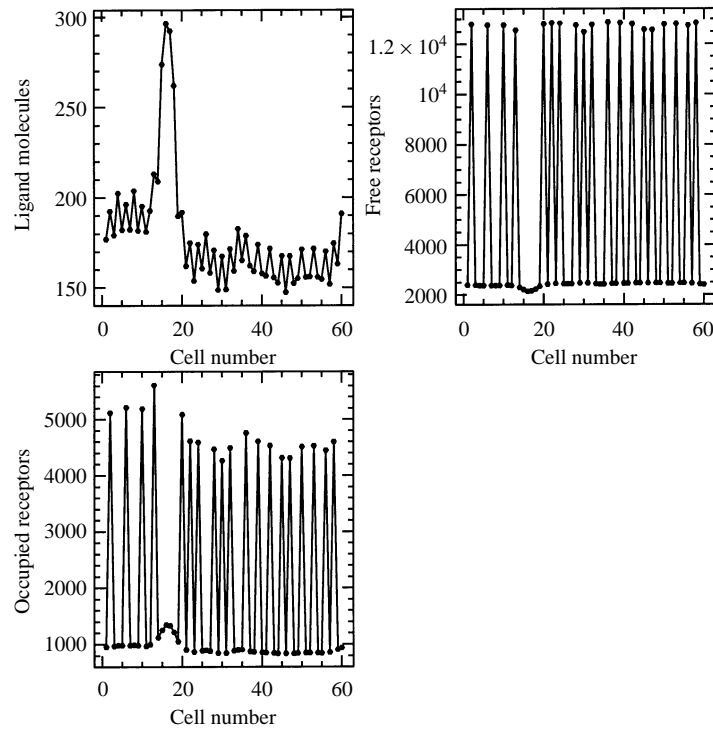


Figure 11. Solution of the nonlinear model for 60 cells. Linear analysis predicts the formation of a pattern with a wavelength between 2 and 56 cells. The pattern we expect to dominate is of mode 2; this wavelength corresponds to the fastest growing mode. The levels of each variable in the solution are quite different from those seen in previous simulations: the peaks in free receptor numbers are double those in Fig. 10, while there is a marked reduction in the number of ligand molecules and bound receptors. Although no regular pattern forms, there are fewer cells between each peak in the number of free and bound receptors. The values of the free parameters in the feedback functions are $C_2 = 2500$, $m = 1.1170$ and $n = 12.3041$. The other parameters are as in Fig. 3. Time $t = 10\,000$ h.

In summary, even with the variety of patterns described above, the mechanism exhibits a robustness throughout the numerical results: each pattern consists of high isolated peaks. In terms of cell development, this means that there are always two distinct fates, one adopted by the cells with high levels of bound receptors and another by their neighbours.

5. DISCUSSION

Previous work has shown that juxtacrine signalling can generate patterns of wavelength 2 cells, as one might expect for a nearest-neighbour mechanism. In particular, Collier *et al.* (1996) studied a discrete model for Delta–Notch signalling during development. Their model is considerably different from ours because of the par-

ticular details of the Delta–Notch system; the model includes lateral inhibition of neighbouring cells via a negative feedback loop involving two variables—in contrast to our three-variable model which has positive feedback. They found that this feedback mechanism only gives rise to patterning with a length scale of one or two cells, which is consistent with the fine-grained patterns seen in a number of developmental processes.

Here we have shown the much more surprising result that, when combined with positive feedback in ligand and receptor expression levels, juxtacrine signalling can generate a wide range of longer wavelength patterns. Linear analysis of our model predicts that patterns of a length scale longer than one or two cells are possible; and we observe such patterns in the numerical simulations. Indeed, patterns with a longer range have been characterized during early development in the fruit fly. One such example is during neuroblast segregation in the *Drosophila* embryo (Skeath and Carroll, 1992). Another is in the developing eye of the *Drosophila*, which consists of a reiterated pattern of 800 unit eyes known as ommatidia. In each ommatidium there are eight photoreceptor neurons or retinula cells. Juxtacrine signalling by the ligand Boss to the receptor Sevenless triggers just one of the retinula cells (R7) to differentiate, enabling the fly to detect ultraviolet light, while the other seven cells adopt different fates (Zipursky and Rubin, 1994). A similar patterning process takes place in the developing eye of the flour beetle *Tribolium* (Friedrich, 1996).

The patterns we observe in our simulations are generated over timescales ranging from hours to days, depending on the strength of the pattern-generating instability. The model we are proposing is generic, and the timescale of pattern formation implied by our parameter values may be inappropriate for particular applications. Indeed, some of the mechanisms involved in early development are likely to be quicker than the binding of TGF α to EGF-R. However, this is a ligand–receptor system for which there exists an extensive amount of empirical data, and in the absence of complete data sets for other juxtacrine signalling molecules, we have used this system in our simulations for consistency.

We have shown that pattern formation in our model for juxtacrine signalling is dependent on parameters of the feedback functions. The linear analysis we carried out to derive the conditions for pattern formation is similar to techniques used by Turing (1952) to investigate diffusion-driven instability in reaction–diffusion systems. Furthermore, the juxtacrine term in our model appears to be similar to the discretized form of one-dimensional diffusion. However, it is the nature of the spatial coupling that distinguishes the patterning mechanism considered in this work from Turing models. For the purposes of this discussion, the average can be written in a more general form, such that

$$\langle a_j \rangle \equiv \frac{a_{j-1} + \mu_1 a_j + a_{j+1}}{\mu_2},$$

for constants μ_1 and μ_2 , where $\mu_1 = 2$, $\mu_2 = 4$ gives the specific form used in our

model. There is an argument for allowing $\mu_1 > 2$, in the case where the molecule acts in both a juxtacrine and autocrine manner. Also, if we set $\mu_1 = 0$ then this corresponds to the purely one-dimensional case of a single row of cells. However the substitution $\mu_1 = -2$, which gives the central difference approximation, would not make sense biologically within the context of our model; likewise $\mu_1 = +2$ does not give the discretized form of a partial derivative. As an aside, we mention that for the case $\mu_1 = 0$, the patterns we observe in numerical simulations (not shown) have one distinct difference from those of our model; the absence of a contribution from cell j to the local average allows peaks of receptors to form in consecutive cells. Another important distinction between the Turing mechanisms and ours is the need for thresholds. Continuum patterning mechanisms require the imposition of thresholds in order to determine cell fate. In contrast, the nature of the patterns generated by our model with their high isolated peaks gives a robust framework for determining cell fate, without the need for such arbitrary levels. Additionally, there are known systems of juxtacrine signalling molecules whereas evidence of diffusing morphogens in developmental biology remains elusive.

There are numerous extensions which could be carried out to the present work. A natural step would be to consider the problem in two dimensions for varying geometrical structures; Collier *et al.* (1996) investigated pattern formation on a hexagonal cellular network. The model itself could be extended to incorporate other biologically relevant features, such as cell movement and cell polarization; the latter could arise from receptors moving on the cell surface while remaining bound within the cell membrane. As mentioned in Section 1, some growth factors that are primarily membrane bound can also be cleaved to give a freely diffusing form; we would therefore need to include some paracrine signalling in the model. This is particularly relevant to signalling via the EGF-R pathway in the developing eye of *Drosophila* (Freeman, 1997).

ACKNOWLEDGEMENTS

HJW was supported in part by an advanced course studentship from the Engineering and Physical Sciences Research Council and in part by a research studentship from the Biotechnology and Biological Sciences Research Council.

REFERENCES

- Benson, D. L., J. A. Sherratt and P. K. Maini (1993). Diffusion driven instability in an inhomogeneous domain. *Bull. Math. Biol.* **55**, 365–384.
- Castets, V., E. Dulos, J. Boissonade and P. DeKepper (1990). Experimental evidence of a sustained standing Turing-type nonequilibrium chemical pattern. *Phys. Rev. Lett.* **64**, 2953–2956.

- Clark, A. J. L., S. Ishii, N. Richert, G. T. Merlino and I. Pastan (1985). Epidermal growth factor regulates the expression of its own receptor. *Proc. Natl. Acad. Sci. USA* **82**, 8374–8378.
- Coffey, R. J., R. Derynck, J. N. Wilcox, T. S. Bringman, A. S. Goustin, H. L. Moses and M. R. Pittelkow (1987). Production and auto-induction of transforming growth factor- α in human keratinocytes. *Nature* **328**, 817–820.
- Collier, J. R., N. A. M. Monk, P. K. Maini and J. H. Lewis (1996). Pattern formation by lateral inhibition with feedback: a mathematical model of Delta–Notch intercellular signalling. *J. Theor. Biol.* **183**, 429–446.
- Dulos, E., J. Boissonade, J. J. Perraud, B. Rudovics and P. DeKepper (1996). Chemical morphogenesis—Turing patterns in an experimental chemical system. *Acta Biophys.* **44**, 249–261.
- Freeman, M. (1997). Cell determination strategies in the *Drosophila* eye. *Development* **124**, 261–270.
- Friedrich, M., I. Rambold and R. R. Melzer (1996). The early stages of ommatidial development in the flour beetle *Tribolium castaneum*. *Dev. Genes Evol.* **206**, 136–146.
- Kauffman, S. A., R. Shymko and K. Trabert (1978). Control of sequential compartment in *Drosophila*. *Science* **199**, 259–270.
- Lewis, J. (1996). Neurogenic genes and vertebrate neurogenesis. *Curr. Opin. Neurobiol.* **6**, 3–10.
- Maini, P. K., K. J. Painter and H. N. P. Chau (1997). Spatial pattern formation in chemical and biological systems. *J. Chem. Soc. Faraday Trans.* **93**, 3601–3610.
- Martiel, J. L. and A. Goldbeter (1987). A model based on receptor desensitization for cyclic AMP signalling in *Dictyostelium* cells. *Biophys. J.* **52**, 807–828.
- Massagué, J. (1990). Transforming growth factor- α : a model for membrane-anchored growth factors. *J. Biol. Chem.* **265**, 21393–21396.
- Massagué, J. and A. Pandiella (1993). Membrane-anchored growth factors. *Ann. Rev. Biochem.* **62**, 515–541.
- Monk, N. A. (1998). Restricted-range gradients and travelling fronts in a model of juxtacrine cell relay. *Bull. Math. Biol.* **60**, 901–918.
- Murray, J. D. (1993). *Mathematical Biology*, 2nd edn, Berlin: Springer-Verlag.
- Murray, J. D., G. F. Oster and A. K. Harris (1983). A mechanical model for mesenchymal morphogenesis. *J. Math. Biol.* **17**, 125–129.
- Murray, J. D., R. T. Tranquillo and P. K. Maini (1988). Mechanochemical models for generating biological pattern and form in development. *Phys. Rep.* **171**, 59–84.
- Olsen, L., J. A. Sherratt and P. K. Maini (1995). A mechanochemical model for adult dermal wound contraction: on the permanence of the contracted tissue displacement profile. *J. Theor. Biol.* **177**, 113–128.
- Oster, G. F., J. D. Murray and P. K. Maini (1985). A model for chondrogenic condensations in the developing limb: the role of extracellular matrix and cell tractions. *J. Embryol. Exp. Morphol.* **89**, 93–112.
- Owen, M. R. and J. A. Sherratt (1998). Mathematical modelling of juxtacrine cell signalling. *Math. Biosci.* **152**, 125–150.

- Owen, M. R., J. A. Sherratt and S. R. Myers (1999). How far can a juxtacrine signal travel? *Proc. R. Soc. Lond. Ser. B* **266**, 579–585.
- Reilly, K. M. and D. A. Melton (1996). The role of short-range and long-range signalling in mesoderm induction and patterning during *Xenopus* development. *Sem. Cell Dev. Biol.* **7**, 77–85.
- Serrano, N. and P. H. O'Farrell (1997). Limb morphogenesis: connections between patterning and growth. *Curr. Biol.* **7**, R186–R195.
- Skeath, J. B. and S. B. Carroll (1992). Regulation of proneural gene expression and cell fate during neuroblast segregation in the *Drosophila* embryo. *Development* **114**, 939–946.
- Turing, A. M. (1952). The chemical basis of morphogenesis. *Phil. Trans. R. Soc. Ser. B* **237**, 37–72.
- Varea, C., J. L. Aragon and R. A. Barrio (1997). Confined Turing patterns in growing systems. *Phys. Rev. E* **56**, 1250–1253.
- Voroney, J. P., A. T. Lawniczak and R. Kapral (1996). Turing pattern formation in heterogeneous media. *Physica D* **99**, 303–317.
- Waters, C. M., K. C. Oberg, G. Carpenter and K. A. Overholser (1990). Rate constants for binding, dissociation, and internalization of EGF: Effect of receptor occupancy and ligand concentration. *Biochem.* **29**, 3563–3569.
- Zigmond, S. H., S. J. Sullivan and D. A. Lauffenburger (1982). Kinetic analysis of chemo-tactic peptide receptor modulation. *J. Cell. Biol.* **92**, 34–43.
- Zipursky, S. L. and G. M. Rubin (1994). Determination of neuronal cell fate: lessons from the R7 neuron of *Drosophila*. *Ann. Rev. Neurosci.* **17**, 373–397.

Received 7 July 1999 and accepted 14 October 1999